Structure and Elastic Properties of 10−12 Pentacosadiyonic Acid Langmuir Films

C. Gourier,*,† M. Alba,‡ A. Braslau,‡ J. Daillant,‡,§ M. Goldmann,§,|| C. M. Knobler,⊥ F. Rieutord,▽ and G. Zalczer‡

Laboratoire de Physique Statistique de l'Ecole Normale Supérieure, 24 rue Lhomond, 75231 Paris Cedex 05, France, Service de Physique de l'Etat Condensé, Commissariat à l'Energie Atomique de Saclay, 91191 Gif-sur-Yvette Cedex, France, Laboratoire pour l'Utilization du Rayonnement Electromagnetique, 91405 Orsay Cedex, France, Objets Complexes et Interfaces d'Intérêt Biologique, Université René Descartes, Paris V, 45 rue René Descartes, 75270 Paris Cedex 06, France, Department of Chemistry and Biochemistry, University of California at Los Angeles, Los Angeles, California 90024-1569, and Commissariat à l'Energie Atomique DRFMC/SI3M, 38054 Grenoble Cedex 9, France

Received December 26, 2000. In Final Form: June 27, 2001

Monolayers of the polymerizable 10−12 pentacosadiyonic acid amphiphile spread on a basic buffer are studied both before and after polymerization. We have established the phase diagram of the unpolymerized Langmuir film by isotherm measurements, Brewster angle microscopy, and grazing incidence X-ray diffraction experiments. Diffuse scattering experiments performed at the European Synchrotron Radiation Facility allowed us to investigate the structure and elastic properties of the different monomer phases and the modifications induced by polymerization.

I. Introduction

Amphiphilic molecules form Langmuir monolayers at air/water interfaces and such films have attracted much attention not only from a fundamental point of view[1] but also with regard to their potential applications after they have been transferred to a solid substrate. These Langmuir−Blodgett films have been employed in fields as different as molecular electronics,[2] integrated optics,[3] and biology.[4] For such applications, good mechanical and thermal stabilities of the systems are required. Those properties can be improved by cross-linking the molecules of the monolayer. The use of diacetylene groups in this context was demonstrated first by Wegner.[5] In our study, we worked with 10−12 pentacosadiyonic acid (PCA), which can form either red- or blue-colored linear polymers under UV radiation due to the diacetylene rod that separates the C_{10} and C_{12} segments of the hydrophobic tail. Films formed by PCA at the air/water interface have already been studied.[6−17]It has been shown that in order to be polymerized, the diacetylenic films have to be at an appropriate density[5,10,11] and the change of color has been related to the molecular density of the film after the polymerization has taken place. A number of UV−visible spectroscopic studies have been performed with the aim of optimizing the irradiation time in order to maximize the extent of polymerization without damaging the film[8,10] or of explaining the change of color.[5,9,11,12] From a structural point of view, comparisons between the molecular organization before and/or after polymerization have been obtained by X-ray reflectivity,[13] electron diffraction,[13,14] and optical microscopy.[14] By controlling the pH of the subphase and the surface pressure, Goettgens et al.[15] tried to optimize the stability and the homogeneity of the PCA monolayers.

Despite all these studies, the 2D phase diagram of PCA is still not well-known. We have therefore undertaken an investigation of the relation between the 2D molecular structure of a PCA monolayer and its elastic behavior before and after polymerization. The article is organized as follows: after the Experimental Section (II) and important details on the film preparation in section III, isotherm studies of PCA spread on a basic buffer are presented in section IV. The effects of the polymerization on the structure and on the elastic properties of PCA films are discussed in sections V and VI. Major conclusions are summarized in section VII.

II. Experimental Section

A. Imaging of the Film: Brewster Angle Microscopy. At the Brewster angle, the reflection coefficient for parallel polarization of light is extremely sensitive to the presence of a film

* Corresponding author: e-mail gourier@lps.ens.fr.
† Laboratoire de Physique Statistique de l'Ecole Normale Supérieure.
‡ CEA-Saclay.
§ LURE.
|| Université René Descartes.
⊥ UCLA.
▽ CEA/DRFMC/SI3M.

(1) Kaganer, V. M.; Möhwald, H.; Dutta, P. *Rev. Mod. Phys.* **1999**, *71*, 779−819.
(2) Sugi, M. *J. Mol. Electron.* **1985**, *1*, 3.
(3) Khanarian, G. *Thin Solid Films* **1987**, *152*, 265.
(4) Reichert, W.; Bruckner, C.; Joseph, J. *Thin Solid Films* **1987**, *152*, 345.
(5) Wegner, G. *Z. Naturforsch.* **1969**, *24B*, 824.
(6) Ringsdorf, H. *J. Polym. Sci.* **1978**, *16*, 12.
(7) Lieser, G.; Tieke, B.; Wegner, G. *Thin Solid Films* **1980**, *68*, 77.
(8) Tieke, B.; Lieser, G. *J. Colloid Interface Sci.* **1982**, *88*, 471.
(9) Tamura, H.; Mino, N.; Ogawa, K. *Thin Solid Films* **1989**, *179*, 33.
(10) Ogawa, K. *J. Phys. Chem.* **1989**, *13*, 5305.
(11) Tomyoka, Y.; Tanaka, N.; Imazeki, S. *Thin Solid Films* **1989**, *179*, 27.
(12) Mino, N.; Tamura, H.; Ogawa, K. *Langmuir* **1991**, *1*, 2336.
(13) Göbel, H.; Kjaer, K.; Als-Nielsen, J.; Möhwald, H. *Thin Solid Films* **1989**, *179*, 41.
(14) Day, D.; Lando, J. *Macromolecules* **1980**, *13*, 1478.
(15) Goettgens, B.; Tillmann, R.; Radmacher, M.; Gaub, H. *Langmuir* **1992**, *8*, 1768.
(16) Huilin, Z.; Weixing, L.; Shufang, Y.; Pingsheng, H. *Langmuir* **2000**, *16*, 2797.
(17) Putman, A.; Hansma, H.; Gaub, H.; Hansma, P. *Langmuir* **1992**, *8*, 3014.

10.1021/la001799v CCC: $20.00
Published on Web 09/19/2001

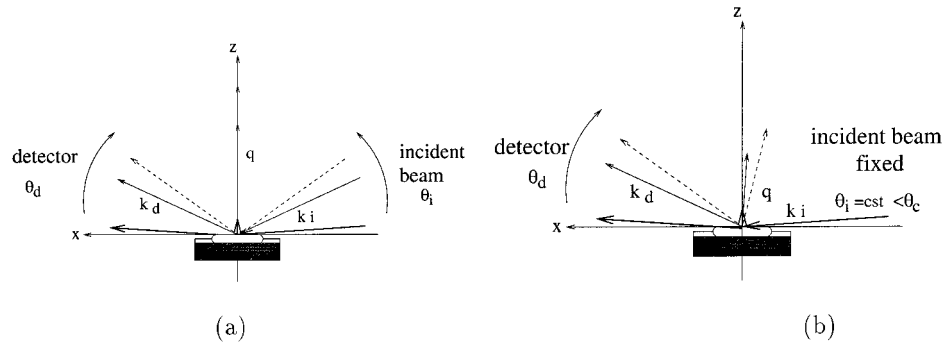

Figure 1. Geometry of (a) reflectivity experiments and (b) diffuse scattering experiments.

even if it is as thin as a monolayer.[18,19]By this principle, the Brewster angle microscope (BAM) from Nanofilm Technology GmbH society allowed us to image in situ (i.e., directly at the air/liquid interface) the shape and texture of monolayer domains of PCA at scales ranged between 10 μm and 1 mm.

B. Grazing Incidence Scattering of X-rays. Grazing incidence scattering of X-rays[20,21] has emerged as a powerful tool for the investigation of the structures and fluctuations of interfaces[22−23] (see ref 24 for a recent review).

The reflection of X-rays impinging on a perfectly flat interface can be determined by the Descartes and Fresnel laws (see for example ref 25). The reflected and transmitted waves are in the plane of incidence (plane defined by the incident light and the normal to the surface, with the angle of reflection equal to the angle of incidence θ_i). For a Langmuir film, an insoluble amphiphilic film at the air/water interface, the modulation of the specularly reflected signal results from the interferences between beams scattered at the different interfaces. At the nanometer scale, no real surface is perfectly flat, and the incident wave is, in fact, not entirely specularly reflected; a small fraction of the intensity is scattered nonspecularly i.e., with scattering angles θ_d different from θ_i or out of the plane of incidence. The off-specular scattering of X-rays can result from density inhomogeneities (as, for example, during a first-order phase transition) but in the present case it is mainly due to height fluctuations. For a monolayer of PCA, the resulting interferences at the five identifiable regions in the density profile (air/chain, chain/diacetylene rod, diacetylene rod/chain, chain/head, and head/subphase) can be calculated within the distorted-wave Born approximation, which takes into account refraction and absorption.[21] The resulting signal gives rise to the modulation of the intensity in the direction of the surface normal and therefore allows the determination of the normal structure of the film.

In this study, two kinds of experiments using small-angle X-ray scattering have allowed the determination of the vertical structure of the amphiphilic films. The first is the usual measurement of the reflectivity, as in ref 13, and the second is a measurement of off-specular (or diffuse) surface scattering, a relatively new technique. The principles of both kinds of experiments are illustrated in Figure 1. For measurements in the plane of incidence, the in-plane q_x and normal q_z wave-vector transfers are given by

$$q_x = \frac{2\pi}{\lambda}(\cos\theta_d - \cos\theta_i)$$

$$q_z = \frac{2\pi}{\lambda}(\sin\theta_d + \sin\theta_i) \qquad (1)$$

where λ is the wavelength and θ_i and θ_d are the angles of the incident beam and the detected beam above the surface.

The reflectivity experiment (Figure 1a) consists of measuring the reflection coefficient of an interface as a function of the out-of-plane wave-vector transfer q_z with the in-plane wave vector q_x equal to zero, i.e., with $\theta_i = \theta_d$. An increase of the incident angle θ_i results in a deeper incident wave penetration and therefore an increase in scattering from the subphase. The detected signal also integrates a diffusely scattered component due to finite-size resolution effects. Since the separation into a specular and a nonspecular part is, in general, not possible, the latter contribution must also carefully be taken into account in order to obtain a correct analysis of the measured reflectivity curves.[21]

The off-specular (or diffuse) surface scattering experiment performed here and illustrated in Figure 1b consists of the measurement of the intensity scattered in the plane of incidence as a function of the wave-vector transfer. In contrast to the reflectivity experiment, the angle of incidence θ_i is kept fixed at a value $\theta_i < \theta_c$, the critical angle for total external reflection. In such an experiment, the normal q_z dependence of the scattered intensity is coupled with the (q_x, q_y) (in-plane modulus of the fluctuation mode) dependence and can be described by the convolution model:[26]

$$I(\mathbf{q}) \propto e^{-q_z^2\langle z^2\rangle} \int dx\, dy\, [e^{q_z^2\langle z(0,0)z(x,y)\rangle} - 1]e^{i(q_x x + q_y y)}\tilde{R}(x,y) \qquad (2)$$

where $\tilde{R}(x,y)$ is the Fourier transform into real space of the angular resolution function. Consequently, the analysis of the nonspecularly diffuse beam should allow not only the determination of the normal structures (it will be interesting to compare the accuracy obtained with both techniques) but also the investigation of the statistical mechanics of out-of-plane fluctuations of amphiphilic interfaces.

Both the interface roughness, characterized in particular by the rms roughness $\langle z^2\rangle$, and the height−height correlation function $\langle z(0,0)z(x,y)\rangle$ can be obtained from the diffuse scattering. The fluctuation spectrum for a fluid interface including the effects of gravity, surface tension γ, and bending rigidity K can be obtained by Fourier transforming the free energy[27,28]and applying the equipartition theorem. It is expected to be given by

$$\langle z(-\mathbf{q})z(\mathbf{q})\rangle = \frac{k_B T}{\Delta\rho g + \gamma(q)q^2 + K(q)q^4} \qquad (3)$$

where the three terms in the denominator respectively describe the limitation of out-of-plane fluctuations by gravity at large scales, by capillarity, and by the bending rigidity modulus at short length scales. Although the validity of eq 3 is still to be demonstrated[23] from an experimental point of view, it has been used in this work to assess the importance of bending effects.

(18) Hénon, S.; Meunier, J. *J. Rev. Sci. Instrum.* **1991**, *62*, 936.
(19) Hönig, D.; Möbius, D. *J. Phys. Chem.* **1991**, *95*, 4590.
(20) Sinha, S. K.; Sirota, E. B.; Garoff, S. *Phys. Rev. B* **1988**, *38*, 2297.
(21) Daillant, J.; Bélorgey, O. *J. Chem. Phys.* **1992**, *97*, 5837.
(22) Braslau, A.; Pershan, P. S.; Swislow, G.; Ocko, B. M.; Als-Nielsen, J. *Phys. Rev. A* **1988**, *38*, 2457−2470.
(23) Gourier, J.; Daillant, A.; Braslau, M.; Alba, K.; Quinn, D.; Luzet, C.; Blot, D.; Chatenay, G.; Grübel, J.-F.; Legrand, G.; Vignaud, C. *Phys. Rev. Lett.* **1997**, *78*, 3157.
(24) Daillant, J.; Alba, M. *Rep. Prog. Phys.* **2000**, *63*, 1725.
(25) Jackson, J. D. *Classical Electrodynamics*, 2nd ed.; J. Wiley and Sons: New York, 1975.
(26) Daillant, J.; Quinn, K.; Gourier, C.; Rieutord, F. *J. Chem. Soc., Faraday Trans.* **1996**, *92*, 505.
(27) Buff, F. P.; Lovett, R. A.; Stillinger, R. H. *Phys. Rev. Lett.* **1965**, *15*, 621−623.
(28) Helfrich, W. *Z. Naturforsch.* **1973**, *28c*, 693−703.

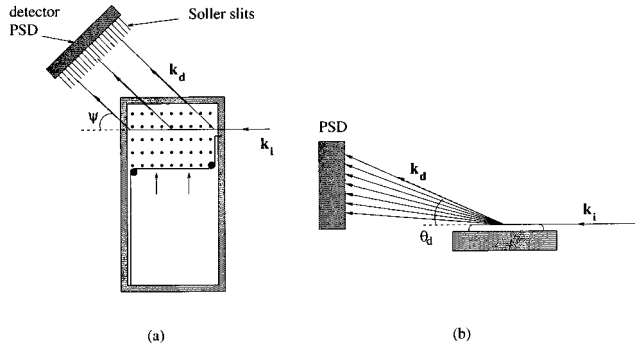

Figure 2. Geometry of diffraction experiments: (a) front view; (b) side view.

Fourier transformation of the fluctuation spectrum given by eq 3 yields the correlation function to be inserted in eq 2:

$$\langle z(0,0)z(x,y)\rangle = \frac{k_B T}{2\pi\gamma}[K_0(r\sqrt{\Delta\rho g/\gamma}) - K_0(r\sqrt{\gamma/K})] \qquad (4)$$

where $r^2 = x^2 + y^2$ and K_0 is the modified Bessel function of second type of order zero. The X-ray reflectivity experiments were performed with the laboratory reflectometer described in ref 29. But, because of the relative complexity of the molecules studied and the limitations of the reflectivity technique, these experiments have only allowed a rough characterization of the vertical structure of the films. The X-ray diffuse scattering experiments were performed at the CRG-IF (BM32) beamline of the European Synchrotron Radiation Facility (ESRF). The desired radiation (λ = 0.0688 nm) was selected by use of the (111) reflections of two silicon monochromator crystals and the angle of incidence on the liquid surface was fixed after reflection by a flat mirror at $\theta_i = 0.85\theta_c$. We took great care to limit the background, as described in ref 26. The beam footprint on the trough was controlled by a primary slit of typical size 0.13 × 1 mm^2, and the resolution was controlled by a pair of slits of typical size 2 × 2 mm^2 and 0.25 × 4 mm^2 positioned, respectively, after the sample (210 mm from the center of the trough) and in front of the detector (720 mm from the center of the trough). We checked on a bare surface of pure water that resolution effects were correctly described by eq 2.

The in-plane structure of the PCA monolayers was determined by grazing angle X-ray diffraction experiments (GIXD)[1] performed at the D24 beamline[30] at the Laboratoire pour l'Utilisation du Rayonnement Electromagnetique (LURE), and the geometry is shown in Figure 2. The incident angle θ_i was also fixed at 85% of the critical angle for total external reflection, and the horizontal wave vector transfer $q_y = (4\pi/\lambda)\sin\psi$ was sampled by changing the horizontal scattering angle ψ.

III. Film Preparation and Isotherm Measurements

The isotherm measurements were performed either in a large homemade Langmuir trough (700 cm^2) adapted to grazing angle X-ray experiments or in a smaller Riegler & Kirstein trough (140 cm^2) that could easily be inserted in a Brewster angle microscope. The surface pressure−area isotherms were measured by continuous compression. The surface tension was measured with a Wilhelmy balance (Riegler & Kirstein), calibrated with the well-known phase transitions (L2−L′2 and L′2−LS) of a behenic acid Langmuir film. The temperature was regulated within ±0.5 °C by a water circulation bath. The troughs were cleaned with nitric acid and acetone, followed by numerous rinses with pure water from a Millipore Milli-Q system (specific resistivity 18.2 MΩ·cm).

Whereas the pure PCA monomer is a white powder, the polymer is blue and forms a red, insoluble suspension in certain organic solvents. It was therefore evident that the PCA, purchased from Lancaster, was always partially polymerized and could not be used as received. To remove the polymer, solutions of PCA were filtered several times before preparation of the spreading solutions. Because of the high reactivity of PCA, the solutions were then stored in the dark at 5 °C.

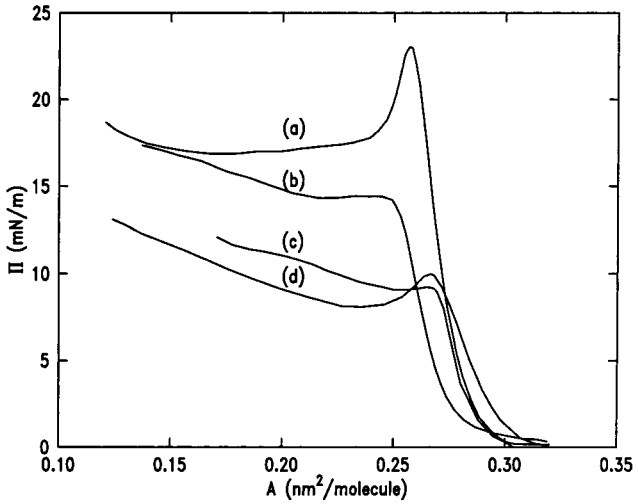

Figure 3. Surface pressure−molecular area isotherms for PCA on pure water subphase at room temperature, with spreading solvent (a) 1:9 ethanol−hexane mixture, (b) chloroform, (c) 1,1,2-trichloroethane, or (d) toluene.

The quality of the films depends significantly on the spreading solvent and the concentration of the spreading solutions. At concentrations higher than 1 mg/mL, nuclei of the bulk phase can be formed during film deposition. On the other hand, the amphiphile can dissolve partially into the subphase at very low concentrations.[31] An ideal spreading solvent must fulfill the following requirements: it has to dissolve the amphiphile, spread it homogeneously over the whole surface, be insoluble in the subphase, be volatile, and be chemically inert. To test solvents with regard to these criteria, isotherm measurements were performed at fixed compression velocity and temperature (4.8 × 10^{-3} nm^2 molecule^{-1} s^{-1}, 19 °C) for various spreading solvents: 1,1,2-trichloroethane, chloroform, toluene, and a 1:9 ethanol−hexane mixture. (A solution with pure 1,1,1-trichloroethane, without stabilizing agents, was also tested but did not spread on water.) The results are shown in Figure 3.

Small shifts (≃0.02 nm^2/molecule) of the molecular area at which the increase in surface pressure occurs can be noticed. They can be attributed either to small concentration errors (defined at ±0.01 mg/mL) in the volume spread or to real physical differences (see below). More interesting is the change in the surface pressure of the low-molecular-area "plateau" of the isotherms, i.e., the collapse pressure at which the film undergoes a transition from a monolayer to a multilayer or a bulk phase. As can be seen in Figure 3, the pressure at which collapse occurs depends on the solvent. For solutions in 1,1,2-trichloroethane and toluene, the collapse pressure of the film is significantly lower than that observed with chloroform or the ethanol−hexane mixture. This may be the result of the poor spreading properties of these two solvents on water. We therefore preferred to use chloroform or a mixture of ethanol and hexane, which spread well. Nevertheless, with chloroform there is a possibility that highly reactive radicals could be formed with a risk of breaking the diacetylene rods[32] and introducing defects into the monolayer.[33] The ethanol−hexane mixture is less reactive, but ethanol is soluble in water, and if care is not taken, a partial solubilization of the amphiphile may occur.[31] The loss of material depends on

(29) Bourdieu, L.; Chatenay, D.; Daillant, J.; Luzet, D. *J. Phys. II (France)* **1994**, *4*, 37.

(30) Fontaine, P.; Goldmann, M.; Rondelez, F. *Langmuir* **1999**, *15*, 1348.

(31) Gericke, A.; Kutscher, J.; Hühnerfuss, H. *Langmuir* **1993**, *9*, 2119.

(32) Peterson, I. Private communication, 1993.

(33) Gourier, C.; Daillant, J.; Chatenay, D.; Knobler, C.; Zalczer, G. Structures of PCA collapsed films. In *Short and long chains at interfaces*; Daillant, J., Guenoun, P., Marques, C., Muller, P., Trân Thanh Vân, J., Eds.; Editions Frontières: Gif-sur-Yvette, France, 1995.

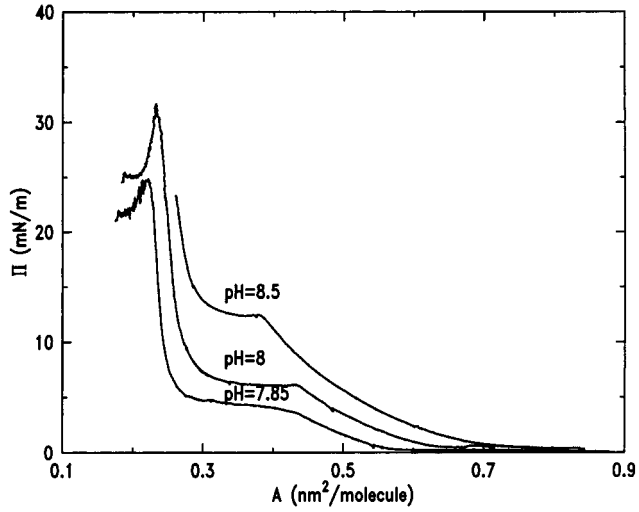

Figure 4. Surface pressure−molecular area isotherms for PCA, with 1:9 ethanol−hexane mixture on sodium tetraborate aqueous subphase: (a) pH = 8.5, (b) pH = 8, (c) pH = 7.85.

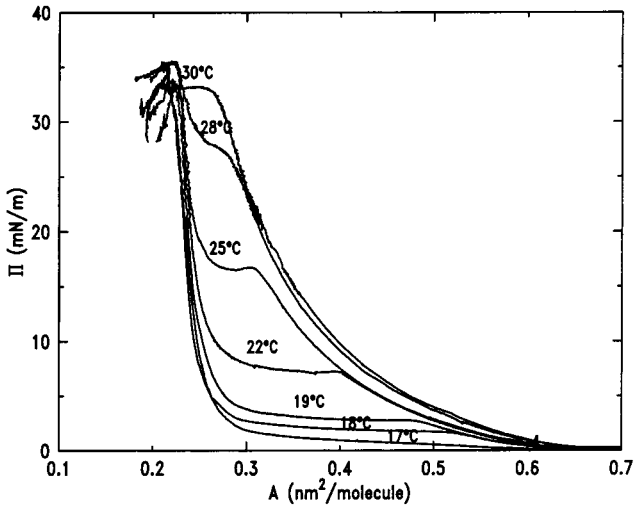

Figure 5. Surface pressure−molecular area isotherms for PCA on a water subphase buffered at pH 7.5 at temperatures ranging between 17 and 30 °C (from bottom to top). The spreading solvent was a 1:9 ethanol−hexane mixture.

the chain length of the amphiphile and on the volumes of the deposited droplets. By using the smallest (10%) fraction of ethanol that allowed a total solubilization of the PCA into the ethanol−hexane mixture, we optimized the spreading technique by carefully creating tiny droplets (1 μL) and letting them gently touch the subphase. When this procedure was followed, no loss was observed in the isotherms (compare Figure 3 panels a and c). Note that with this procedure there is a bump in the isotherm at high pressure, which is indicative of a nucleation barrier. It is much less pronounced with the other solvents, indicating that nuclei are either already present or much easier to nucleate with trichloroethane, toluene, or chloroform. All further experiments presented in this work have then been performed with the 1:9 ethanol−hexane spreading solvent.

Another important parameter is the nature of the subphase. For PCA, we have observed that on pure water the monolayer is unstable and collapses. It has been observed[15] that the monolayer can be stabilized with respect to collapse to bilayers or multilayers by spreading on a basic subphase. The PCA headgroups ionize at high pH and a repulsive force appears between them consistent with the fact that sheets in the multilayer stack would repel each other. This phenomenon is illustrated in the isotherms shown in Figure 4, which are consistent with those reported by Goettgens et al.[15] Although the collapse pressure increases with increasing pH, it also becomes more difficult to reach the smaller molecular areas necessary for polymerization. For this reason, we chose to carry out our experiments on a subphase maintained at pH 7.5 by a sodium tetraborate buffer.

IV. Isotherm Studies

Isotherms of PCA spread on a sodium tetraborate buffer at pH 7.5 at temperatures ranging between 17 and 30 °C are shown in Figure 5. The form of the isotherms is reminiscent of that of simple fatty acids or phospholipids on pure water.[34,35]The transition plateau reveals the presence of at least two distinct phases. An evaluation of the compressibilities of these phases can be obtained by the relation

$$\chi_T = -\frac{1}{A}\left(\frac{\partial A}{\partial \Pi}\right)_T \qquad (5)$$

One has to note that if the monolayer is inhomogeneous (we will see from the BAM studies that this is indeed the case), eq 5 will only give a rough approximation of the real compressibility.[36] Starting from $\Pi = 0$ mN/m at large molecular areas, there is a slow increase of the surface pressure that is the signature of a very compressible phase (40 m/N), with molecular area $A \gg 0.7$ nm^2; we will call this the expanded phase. There is then a plateau characteristic of a first-order transition from the expanded phase to a denser phase (condensed phase). After the transition is completed, the compression of the condensed phase gives rise to a steep increase in pressure. The compressibility of this phase (2.4 m/N) is about 16 times smaller than that of the expanded phase. The monolayer undergoes collapse at 33 ± 1 mN/m (0.215 ± 0.015 nm^2).

The PCA film was exposed to UV radiation both in the expanded phase and in the condensed phase, with the help of a commercial Hg vapor lamp ($\lambda = 254$ nm), under argon atmosphere to protect the film from ozone oxidation. The UV irradiation was stopped after a few minutes to avoid any alteration of the polymerized layer, easily revealed by an increase in surface pressure. Powdered sulfur was deposited on the film to visualize its flow under a gentle stream of air. After the irradiation, no motion of the condensed phase could be observed; the film appears to be rigid. In addition, the appearance of a pale pink color of the layer after irradiation is typical of the polymerized PCA.[6,9,11] In contrast, there was no evidence of any long-range polymerization after irradiation of the expanded phase. The layer remained as fluid as before exposure, and no pink color could be observed. This suggests that the polymerization of PCA films is a selective process with respect to the structure of the monolayer, in agreement with the often quoted topochemical nature of the polymerization reaction.[15,17,29] If the surface pressure of the condensed phase is kept constant during irradiation, the molecular area of the film is reduced by about 10%. Similarly, if the average molecular area is kept fixed during the polymerization, there is a decrease in surface pressure. Both observations suggest a rearrangement of the molecules within the film. The often proposed (but rarely checked) explanation is the contraction of the two-dimensional molecular network[7,14] during polymerization. We note finally that the polymerized film can be com-

(34) Albrecht, O.; Gruler, H.; Sackmann, E. *J. Phys. (Paris)* **1978**, *39*, 301.

(35) Ulman, A. *An Introduction to Ultrathin Organic Films: from Langmuir−Blodgett to Self-Assembly*; Academic Press: New York, 1991.

(36) Fradin, C.; Daillant, J.; Braslau, A.; Luzet, D.; Alba, M.; Goldmann, M. *Eur. Phys. J. B* **1998**, *1*, 57−69.

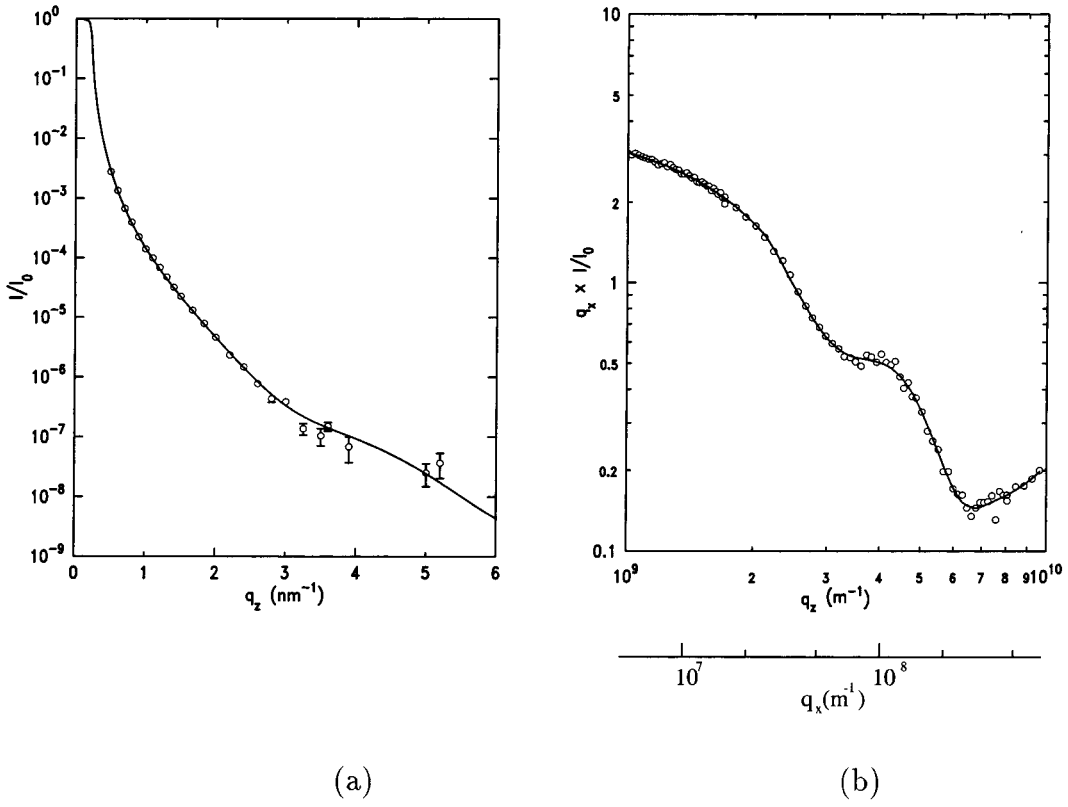

Figure 6. (a) X-ray reflectivity curve recorded at room temperature in the expanded phase at 0.6 nm^2/molecule and a pressure of 3 mN/m. (b) X-ray diffuse scattering curve recorded at room temperature in the expanded phase at 0.55 nm^2/molecule and a pressure of 3 mN/m.

pressed to a much higher pressure than the unpolymerized film (>40 mN/m) without collapsing.

V. Structural Study

A. Expanded Phase. The expanded phase could not be detected with our Brewster angle microscope. In addition, at 22 °C and for a molecular area equal to 0.5 nm^2, no molecular structure could be observed by GIXD experiments. Both results confirm that, as expected from the isotherm measurements and UV irradiation, the expanded phase is not organized. To characterize the vertical structure of the molecules in the expanded phase, X-ray reflectivity experiments were carried out with the laboratory reflectometer (Figure 6a), and X-ray grazing incidence diffuse scattering experiments (Figure 6b) were performed at the ESRF.

We first discuss the shape of these curves. In the normalized reflectivity data curve (Figure 6a), beyond $q_z = 4 \times 10^9$ m^{-1}, the signal coming from the monolayer, about 10^7 times less intense than the incident beam, is no longer perceptible. This is not the case for the diffuse scattering data (Figure 6b), which allow the detection of a weaker signal (10^{-8} times the incident beam intensity). This extension of the measurements toward larger wave vectors ($q_z = 6 \times 10^9$ m^{-1}) provides a better accuracy on the determination of the structural parameters. This new and more efficient method of investigation of the normal structure of a film is, in our opinion, one important result of this work. Moreover, the grazing angle of incidence need not be changed during an experiment, which is a great advantage when synchrotron radiation is used. The experiment is then much easier to carry out since the angle of incidence can be fixed with a simple mirror instead of a complicated beam deflector.

It is interesting to note that synchrotron reflectivity experiments did not give much better results than those performed in the laboratory with a sealed tube source. In fact, the better results obtained in the X-ray diffuse scattering geometry are mainly due to the effect of the limitation of the bulk scattering thanks to an incident angle fixed below the critical angle of total external reflection. Even though systematic reflectivity experiments were performed on the laboratory reflectometer, emphasis will be put on the diffuse scattering data obtained on the BM32 beamline. In Figure 6b, I/I_0 has been multiplied by q_x in order to reduce the ordinate scale to 2 orders of magnitude instead of the 8 orders obtained experimentally, which allows a better view of details.

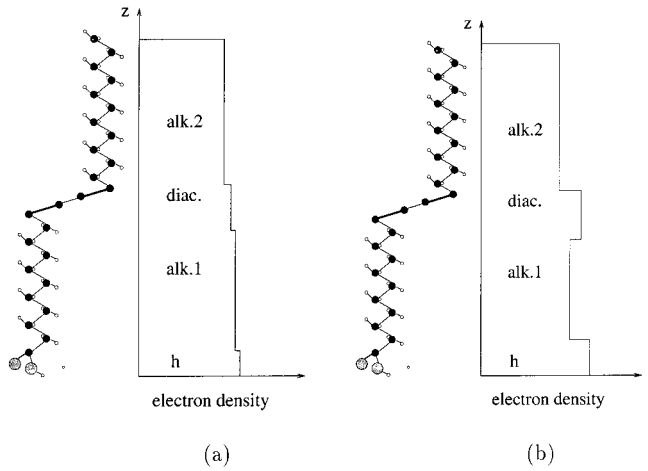

Figure 7. Schematic of the model used to fit the X-ray experimental data (a) in the case of the expanded phase and (b) in the case of the condensed phase and the polymerized film.

The experimental data were fit with a four-box model (Figure 7a): one for the upper alkyl chain (thickness l_{alk_2},

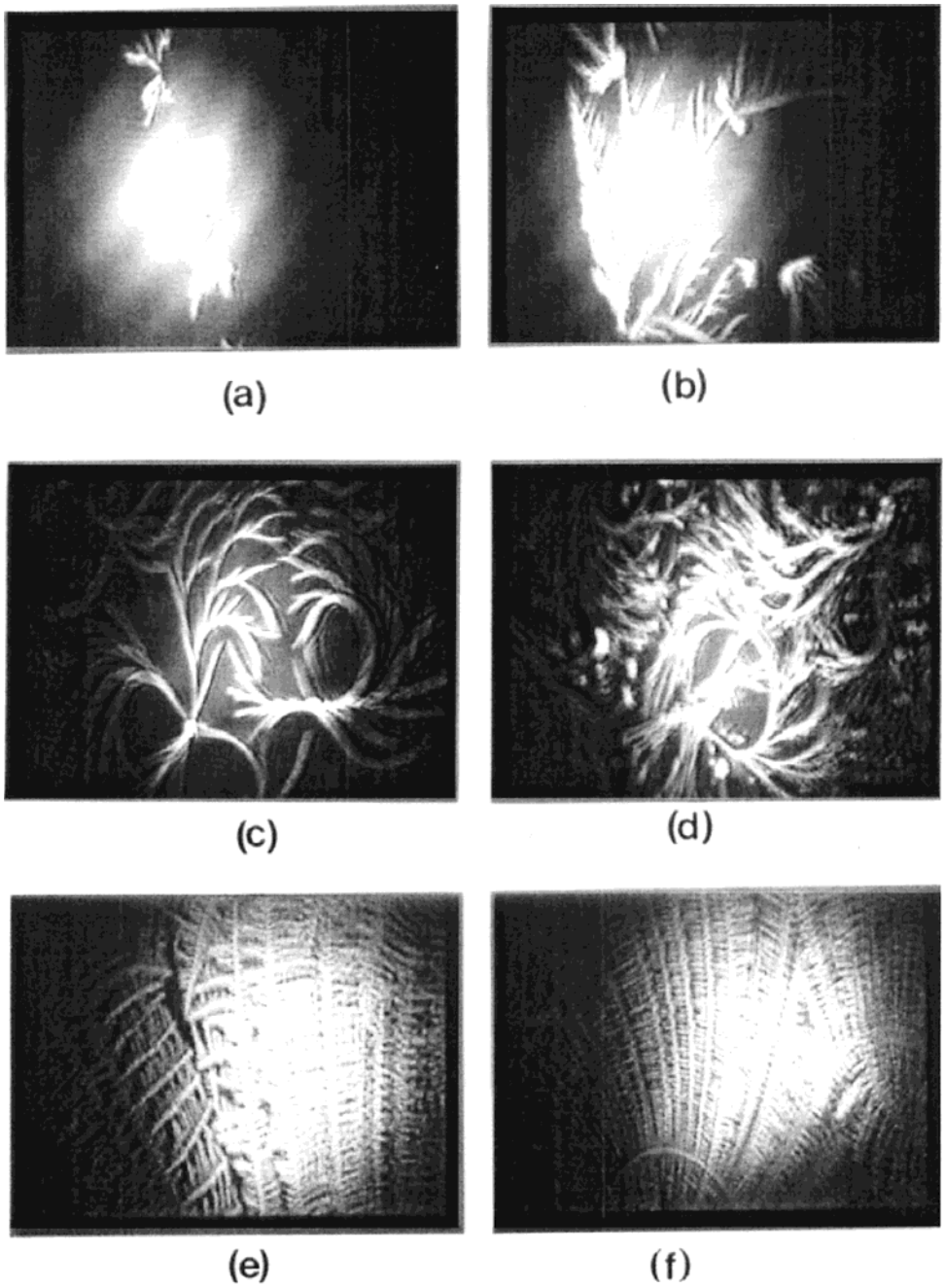

Figure 8. Brewster angle microscopy images (600 × 400 μm^2) of the evolution of the PCA film with the molecular area and surface pressure: (a) nucleation of the condensed phase, (b) condensed phase, (c, d) growth from 3-D nuclei, (e, f) ordered condensed phase.

electron density ρ_{alk_2}), one for the diacetylene rod (thickness l_{diac}, electron density ρ_{diac}), one for the lower alkyl section (thickness l_{alk_1}, electron density ρ_{alk_1}), and one for the COOH headgroup (thickness l_h, electron density ρ_h). According to the fit, the overall thickness of the monolayer is about 1.86 nm, with $l_{alk_2} = 0.86$ nm, $l_{diac} = 0.25$ nm, $l_{alk_1} = 0.50$ nm, and $l_h = 0.25$ nm. The lengths obtained from this kind of experiment are projections over an axis normal to the interface. Thus, since the total thickness we measure is small compared to the thickness of the fully stretched molecule (3.1 nm), it implies that the chains must be highly tilted and/or disordered in the expanded phase. For the electron densities, the parameters of the fit are $\rho_{alk_2}/\rho_{water} = 0.85$, $\rho_{diac}/\rho_{water} = 0.93$, $\rho_{alk_1}/\rho_{water} = 1.04$, and $\rho_{head}/\rho_{water} = 1.10$. This progressive decrease of the densities, from the acid head on the subphase to the upper alkyl chains, is again indicative of a disordered expanded phase. The role of the diacetylene rods will be examined in section V(D). Let us finally mention that the surface tension given by the model is consistent with the value directly obtained from the Wilhemy balance measurement.

B. Condensed Phase. *a. Texture.* As previously mentioned, coexistence between the expanded phase and a condensed phase takes place upon compression. In contrast to the expanded phase, the nucleation (Figure 8a) and growth (Figure 8b,e,f) of the condensed phase could be observed with BAM. By carefully controlling the pH and the temperature, a condensed phase with very long-range ramified structures (>1 mm) was systematically observed (Figure 8e,f). These domains are highly ordered. This texture could be the one leading to the well ordered polymer of ref 15. Upon further compression, the condensed domains come into contact. Nevertheless no deformation could be observed at the 10 μm scale, which is the resolution of our BAM. If the stress becomes too great, the film collapses, and three-dimensional bright

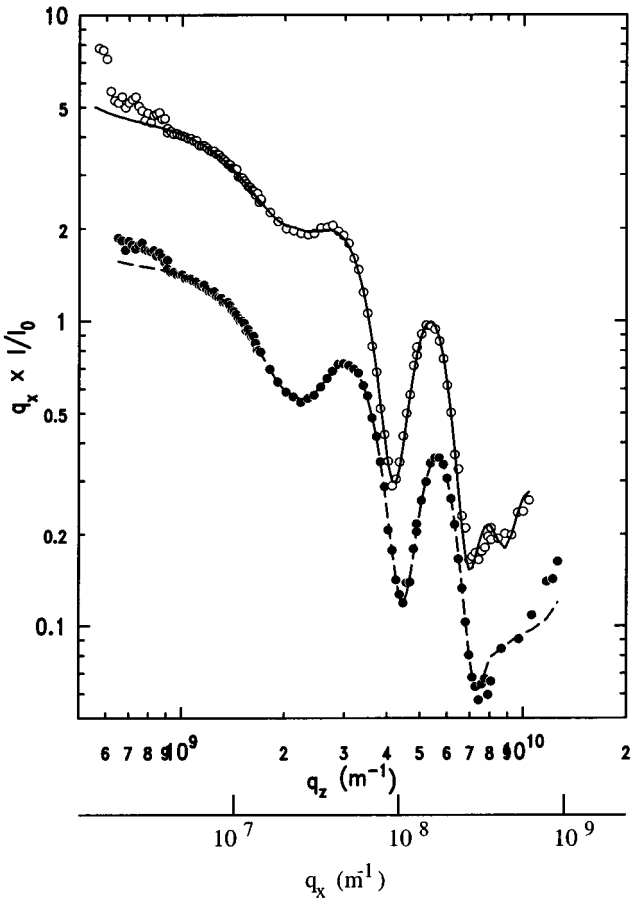

Figure 9. X-ray diffuse scattering: (●) condensed phase $\pi =$ 10 mN/m, $A = 0.29$ nm^2/molecule; (○) polymerized monolayer at $\pi = 10$ mN/m, $A = 0.27$ nm^2/molecule. For clarity, q_xI/I_0 versus q_x is shown and the ordinate axis for the condensed phase is divided by 3.

nuclei appear (Figure 8c,d). Except for these bright nuclei, if any, the domains slowly melt upon decompression. The expanded−condensed phase transition is reversible. The behavior of the condensed domains upon compression, the long-range order, and the inhomogeneities are reminiscent of those of a solid.

b. Vertical Plane Structure. Once again, to study the vertical structure of the condensed phase, reflectivity and diffuse scattering experiments were performed. As previously explained, better results are obtained with the diffuse scattering experiments. Figure 9 (b) shows the measured diffuse spectrum of the film at 22 °C and compressed to $\Pi = 10$ mN/m, $A = 0.29$ nm^2 obtained with this technique. As in the case of the expanded phase, the data were fitted with a four-box model. In this case, however, the height of the headgroup obtained from the best fit corresponded to the carboxyl group including the first methylene rather than the -COOH group alone (Figure 7b). One can note that the electron density is no longer a decreasing function of the distance from the subphase, as it was for the expanded phase. From the fit parameters given in Table 1, we can estimate the molecular area layer by layer from the simple expression $A = N_e/t\rho$, where t is the thickness of the layer and ρ is its electron density, and where the number of electrons is taken equal to $N_e(\text{alk}_2) = 89$, $N_e(\text{diac}) = 24$, $N_e(\text{alk}_1) = 64$ and $N_e(\text{h}) = 31$. The molecular areas are $A(\text{alk}_2) = 0.22$ nm^2, $A(\text{diac}) = 0.23$ nm^2, $A(\text{alk}_1) = 0.26$ nm^2, and $A(\text{h}) = 0.22$ nm^2. From the near constancy of these areas and the marked profile in the electron density, it is evident that the condensed phase is structured.

Table 1. Fit Parameters of X-ray Diffuse Scattering Experiments Recorded on the Condensed Phase and on the Polymerized Monolayer[a]

	condensed phase	polymerized monolayer
γ (mN/m)	63	63
$\rho_{\text{alk}_2}/\rho_{\text{water}}$	0.93 ± 0.01	0.92 ± 0.01
$\rho_{\text{diac}}/\rho_{\text{water}}$	1.08 ± 0.02	1.26 ± 0.03
$\rho_{\text{alk}_1}/\rho_{\text{water}}$	0.96 ± 0.02	0.96 ± 0.02
$\rho_{\text{h}}/\rho_{\text{water}}$	1.27 ± 0.02	1.24 ± 0.02
l_{alk_2} (nm)	1.27 ± 0.02	1.29 ± 0.03
l_{diac} (nm)	0.28 ± 0.02	0.18 ± 0.02
l_{alk_1} (nm)	0.73 ± 0.02	0.96 ± 0.03
l_{h} (nm)	0.32 ± 0.02	0.30 ± 0.03
K (k_BT)	250 ± 100	500 ± 100

[a] Buffer pH was 7.5.

c. In-Plane Structure. To explore the two-dimensional crystallinity of the condensed phase, we have performed GIXD experiments (LURE−DCI). Figure 10a shows the diffraction pattern of a monolayer compressed at a surface pressure $\pi = 20$ mN/m, at 22 °C. Two distinct in-plane diffraction peaks were observed in the measured range (1 Å^{-1} < q_{xy} < 2.6 Å^{-1}): one at 1.38 ± 0.01 Å^{-1} and the other one at 1.50 ± 0.01 Å^{-1}. The location of the peaks was determined by fitting the curves to Lorentzians. These singularities demonstrate that the condensed phase has 2D order. Nevertheless the diffraction pattern is consistent with an oblique cell of area $A = 4\pi^2/(q_{01}q_{10} \sin \alpha)$ with $q_{10} = 1.38$ Å^{-1}, $q_{01} = q_{-11} = 1.50$ Å^{-1}, and $\alpha \simeq 62°$, α being the complementary angle to the one between the two vectors a_{10} and a_{01} (unconventional indexation, see Figure 10b), assuming that there is only one molecule per unit cell and that the molecular area obtained from the diffuse scattering curve ($A \simeq 0.22$ nm^2) is a good estimate of the area of the diffraction unit cell. A cell angle close to 60° is characteristic of close packing of the aliphatic chains due to attractive van der Waals interactions, but the asymmetry of the PCA molecule is not compatible with a fully compact structure. The observed deviation from a hexagonal cell leads us to propose that the diacetylene rods are aligned along the larger cell parameter (i.e., a_{10}) in the condensed phase (see Figure 11a).

C. Polymerized Film. *a. Vertical Plane Structure.* Figure 9 allows the comparison of the diffuse scattering curves of the same PCA film before (●) and after (○) polymerization at a pressure $\Pi = 10$ mN/m. Upon polymerization, the film thickness increases (from 2.60 to 2.73 nm) whereas the thickness of the diacetylene rods decreases (Table 1). The latter observation is explained by the fact that the polymerization imposes a horizontal average position to the diacetylene rods, as illustrated in Figure 12. The increase of the film thickness suggests a decrease of the molecular area and of the in-plane lattice constants. From the fit parameters (Table 1), we can perform the same calculation of the molecular areas as for the unpolymerized film. We obtain $A(\text{alk}_2) = 0.22$ nm^2, $A(\text{diac}) = 0.31$ nm^2, $A(\text{alk}_1) = 0.20$ nm^2, and $A(\text{h}) = 0.20$ nm^2. The small diacetylene rod thickness is responsible for the great difference between the area associated with the diacetylene layer and the others. Nevertheless, the relative error made in this small value is large. Therefore, if we do not take into account the diacetylene layer, the molecular area of the PCA film is appreciably smaller after polymerization. This observation is also consistent with the surface pressure decrease occurring upon polymerization (see Section IV).

b. In-Plane Structure. GIXD experiments have been performed at LURE on the film, after UV irradiation in the condensed phase during a few minutes at constant area (0.25 nm^2/molecule, $t = 22$ °C). The polymerized film

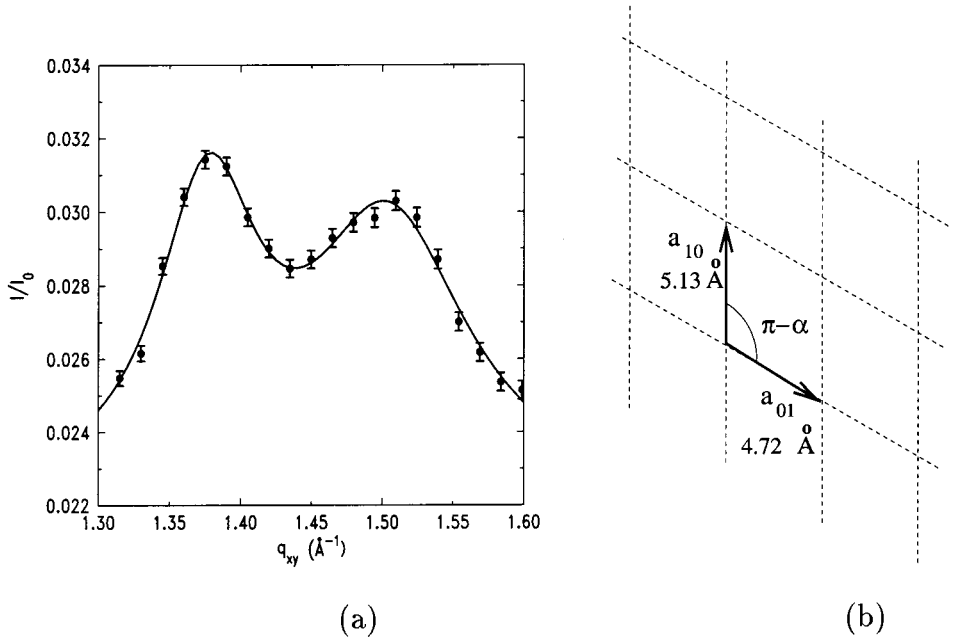

Figure 10. (a) X-ray diffraction curve of the condensed phase at $\pi = 20$ mN/m. (b) Schematic of the associated oblique unit cell: $a_{10} = 5.13$ Å^{-1}, $a_{01} = 4.72$ Å^{-1}, and $\alpha \simeq 62°$.

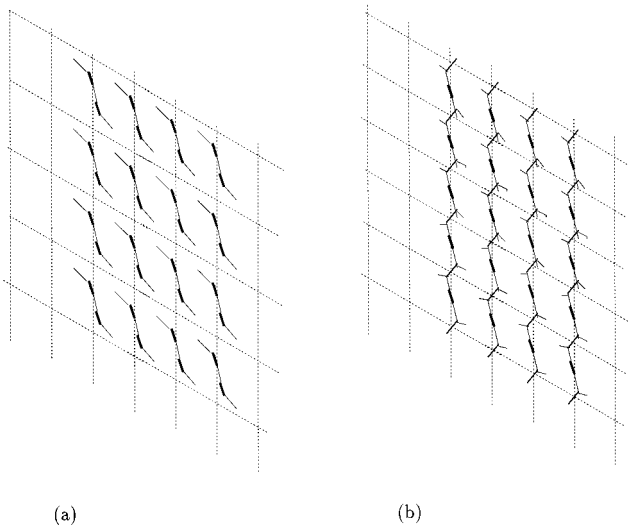

Figure 11. Scheme of the polymerization process (front view): (a) before polymerization; (b) after polymerization.

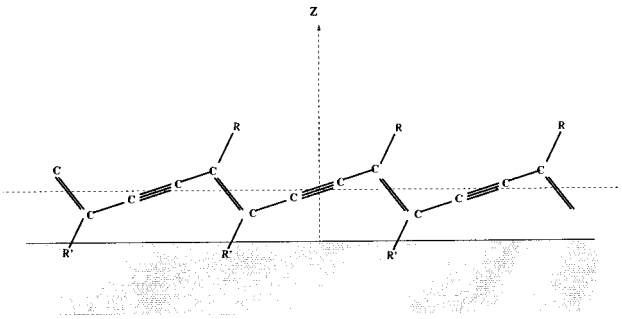

Figure 12. Schematic of a linear polymer of PCA on the subphase (side view). The average position of the diacetylenic rod is horizontal.

gives rise to two peaks at 1.473 ± 0.010 and 1.545 ± 0.010 Å^{-1} (Figure 13a) plus one much weaker Bragg singularity at 2.55 ± 0.02 Å^{-1} (not shown in the figure). Thanks to this last singularity, the three peaks could be indexed with confidence as q_{10} for the first one, q_{01} and q_{-11} for the second degenerated one, and q_{11} ($q_{11}^2 = q_{01}^2 + q_{10}^2 - 2q_{01}q_{10}\cos 2\alpha$) for the last one. The dimensions of the associated oblique unit cell (Figure 13b) are $a_{10} = 5.05$ Å, $a_{01} = 4.81$ Å, and $\alpha = 58°$ (Figure 13b), and its area of 0.205 nm^2 is consistent with the value deduced from diffuse scattering experiments. From these results, it is interesting to note that during polymerization, the lattice area shrinks by about 10% (the molecular area was around 0.23 nm^2 before polymerization). This contraction not only explains the decrease of pressure observed when the average molecular area is kept constant during UV irradiation but also is fully consistent with the decrease in the average molecular area recorded on isotherm measurements when the polymerization is done at constant pressure. A possible scheme of polymerization of the PCA monolayer is proposed in Figure 11.

Göbel et al.[13] examined the changes upon polymerization of the vertical structure in monolayers of a two-tailed diacetylenic lipid [dimethylbis(2-hexacosanoic-10,12-dinoyl)oxaethylammonium bromide, "Bronco"] by X-ray reflectivity and determined the in-plane structure by GIXD. They also observed an increase in the thickness of the film upon polymerization and attributed it to a decrease in the tilt angle. (In their analysis they imposed the constraint that the electron densities in the two alkane segments be the same and that the lengths of the chains be proportional to the number of methylenes, which rules out the possibility of different extent of disorder in the two segments.) They carried out GIXD measurements, and electron diffraction studies only on polymerized films.

D. Influence of the Diacetylenic Rod. The thicknesses of PCA monolayers in the expanded phase and in the condensed phase are small compared with those of fatty acids of comparable molecular weight such as behenic and melissic acid.[37] This suggests that the chains are either disordered or tilted in PCA films. The reason is probably partly due to the diacetylene rods, which introduce an asymmetry in the molecule and divide the alkyl chains into two relatively short segments (C_{10} and C_{12}). The van der Waals attractions between each of these segments

(37) Daillant, J.; Bosio, L.; Harzallah, B.; Bénattar, J. J. *J. Phys. II (France)* **1991**, *1*, 149.

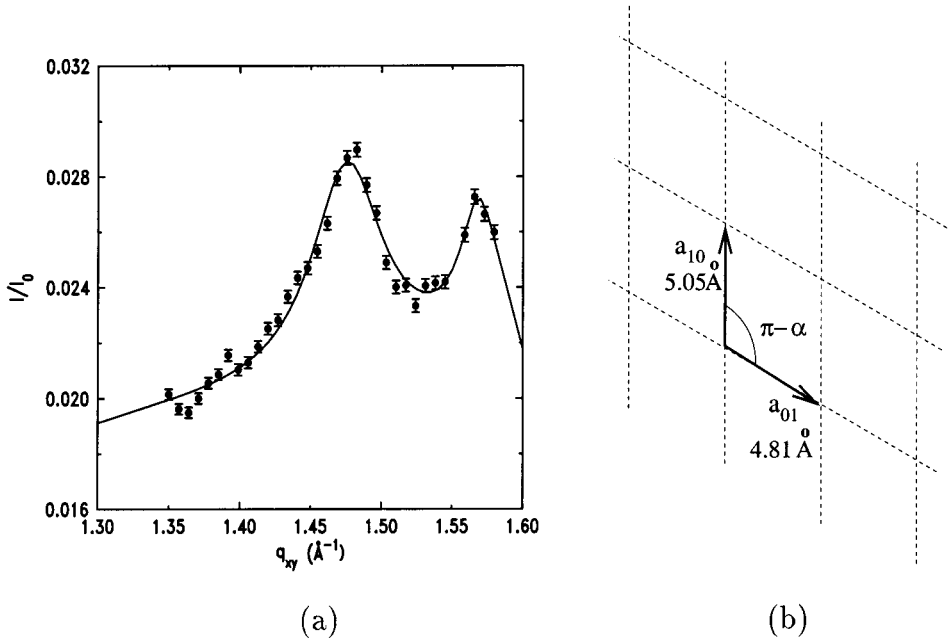

Figure 13. (a) X-ray diffraction curves of a polymerized monolayer of PCA. (b) Schematic of the associated oblique unit cell: $a_{10} = 5.05$ Å^{-1}, $a_{01} = 4.81$ Å^{-1}, and $\alpha \simeq 58°$.

contributes to the stability of the PCA films but probably not enough to compensate for the entropic effects[8] (amplified by the possibility for the diacetylene rod to rotate round the axis of the alkyl chains). Moreover, it is interesting to note that the difference between the thicknesses of the expanded and condensed phases is more important than that between the two phases in fatty acid monolayers.[37] The thickness of PCA films is very sensitive to external conditions and particularly to the surface pressure. Once again, the asymmetry introduced by diacetylene rods in the molecule is probably responsible for this effect. It provides the upper and lower alkyl chains the flexibility needed to change the monolayer structure upon compression. To finish with the role of the diacetylene rod, we recall that the condensed phase of PCA was found to be favorable to the polymerization reaction. According to the previous discussion, diacetylene compounds with diacetylene rods near the acid head should make effective ordered condensed phases because of stronger van der Waals interactions. Nevertheless, such stable assemblies do not guarantee a good polymerization reaction.[8] As we have shown, the polymerization process requires a rearrangement of the molecules. In contrast with a more stable ordered phase, the flexibility of the PCA chains in the condensed phase allows such a rearrangement.

VI. Elastic Properties

A. Bending Rigidity. The scattering by the expanded and condensed PCA films was fitted to the fluctuation spectrum of eq 3 including a Kq^4 term. The sensitivity of the experiment is approximately $\gamma/{q_{x_{max}}}^2$, where $q_{x_{max}}$ is the position of the last interference maximum. Despite the care taken to limit the background, the effective wavevector range where K has a limiting effect on the fluctuation spectrum remains quite restricted. This is due to the small value of $\sqrt{K/\gamma}$ for films spread at the air/water interface. Nevertheless, a high value of the bending rigidity modulus $K = (250 \pm 100)k_BT$ was unambiguously necessary to fit the condensed-phase spectrum, whereas the curve recorded for the expanded phase could be fit with a much lower bending rigidity (a few times k_BT). This expected increase[37] in K when the compressibility of the film decreases has recently been observed with the same technique for an arachidic acid monolayer spread on a pure water subphase.[23]

In the case of the polymerized PCA film, the covalent bonds between the molecules stiffen the monolayer, as revealed by the larger value of the bending rigidity modulus [$K = (500 \pm 100)k_BT$] required to fit its fluctuation spectrum (Figure 9, O).

B. Buckling of the Polymerized Monolayer. Finally, the intensity scattered in the plane of incidence (x, z) by a highly compressed polymerized monolayer is presented in Figure 14b as a function of the longitudinal wave vector transfer q_x at $q_z = 0.5$ nm^{-1}. In this experiment, performed with the laboratory diffractometer, both θ_i and θ_d change in order to keep q_z constant (Figure 14a). The central peak at $q_x = 0$ corresponds to the specular condition. More interesting are the broad peaks observed at $q_x = \pm(3 \times 10^{-3})$ nm^{-1}, which are absent in all of the scattering curves of unpolymerized PCA film before it collapses. These singularities reveal a well-defined wavelength in the polymerized system ($\lambda = 2\pi/q_x \approx 2$ μm) that can be attributed either to height fluctuations or to density inhomogeneities within the film. The latter possibility is not consistent with the fact that this excess scattering is not observed with the unpolymerized film, which is as inhomogeneous as the polymerized one. Moreover, the bending rigidity of the polymerized film is larger and it can be compressed without collapsing to a much larger pressure than the unpolymerized film (>40 mN/m). We interpret this excess scattering as being associated with a buckling of the overcompressed polymerized film in the vertical direction. This process is the only one that would allow a relaxation of the stresses as other mechanisms of collapse are not possible because of the covalent bonds. Buckling of a polymerized octadecyltrichlorosilane monolayer at the air/water interface[38] and of a solid phospholipid phase on a formamide subphase[39] have already been observed in the same range of in-plane vector transfer. Recently, diffuse scattering techniques have been suc-

(38) Bourdieu, L.; Daillant, J.; Chatenay, D.; Braslau, A.; Colson, D. *Phys. Rev. Lett.* **1994**, *72*, 1502.
(39) Saint-Jalmes, A.; Gallet, F. *Eur. Phys. J. B* **1998**, *2*, 489.

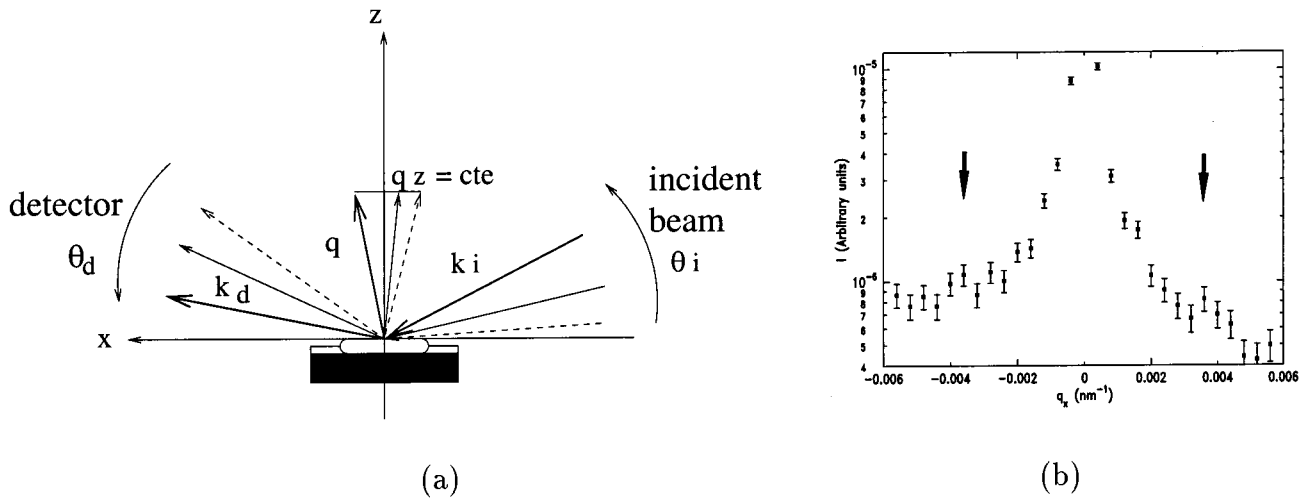

Figure 14. (a) X-ray diffuse scattering experimental configuration in which the intensity is scattering in the incidence plane (x, z) while $q_z = 0.5$ nm^{-1} remains constant. (b) X-ray diffuse scattering curve observed on a highly compressed polymerized monolayer. The arrows indicate the position of the diffusion due to the buckling of the film.

cessfully applied to study the buckling induced by the adsorption of charged copolymers at the air/water interface,[40] and we can conclude that it would be very interesting to perform such experiments on overcompressed polymerized PCA films.

VII. Conclusion

In conclusion, the study of the structure and elastic properties of 2D PCA films, spread on a basic buffer, before and after polymerization by UV irradiation, has been exposed in this article. The expanded phase was found to be a very compressible, non ordered and non polymerizable 2D phase. Thanks to the Brewster angle imaging technique, the nucleation and the growth of the condensed phase have been observed in situ. By carefully controlling the temperature and the pH, very long range inhomogeneous but highly ordered domains were observed. Exposed to UV light, the condensed phase gives rise to a polymerized monolayer. X-ray scattering experiments performed either on the laboratory reflectometer, on the BM32 beamline at ESRF, or on the D24 beamline at LURE have allowed the investigation of the vertical structure and of the in-plane crystalline structure of the monolayer before and after polymerization. An important result of the work is the demonstration that the normal structure of monolayer films can be determined efficiently and precisely from the diffuse scattering. The contraction of the 2D molecular network during polymerization has been proved and a polymerization process has been suggested. The high bending rigidity necessary to fit the X-ray diffuse scattering experiments performed on the polymerized monolayer gives evidence of the stiffening of the layer due to the covalent bonds formed between the molecules of PCA during the polymerization. Finally, when it is highly compressed, the polymerized film has been found to buckle in the third dimension.

Acknowledgment. This study has benefited from financial support from the NATO organization. We thank C. Blot and D. Luzet for indefectible support.

LA001799V

(40) Fontaine, P.; Daillant, J.; Guenoun, P.; Alba, M.; Braslau, A.; Mays, J.; Petit, J. M.; Rieutord, F. *J. Phys. II (France)* **1997**, *7*, 401.